Journal of Structural Biology **136,** 227–238 (2001)
doi:10.1006/jsbi.2002.4442, available online at http://www.idealibrary.com on IDEAL®

An Automatic Particle Pickup Method Using a Neural Network Applicable to Low-Contrast Electron Micrographs

Toshihiko Ogura and Chikara Sato

Neuroscience Research Institute, National Institute of Advanced Industrial Science and Technology (AIST), Tsukuba, Ibaraki 305-8568, Japan

Received October 31, 2001, and in revised form January 29, 2002

Three-dimensional reconstruction from electron micrographs requires the selection of many single-particle projection images; more than 10 000 are generally required to obtain 5- to 10-Å structural resolution. Consequently, various automatic detection algorithms have been developed and successfully applied to large symmetric protein complexes. This paper presents a new automated particle recognition and pickup procedure based on the three-layer neural network that has a large application range than other automated procedures. Its use for both faint and noisy electron micrographs is demonstrated. The method requires only 200 selected particles as learning data and is able to detect images of proteins as small as 200 kDa. © 2002 Elsevier Science (USA)

Key Words: **single-particle analysis; neural networks; automatic particle pickup; cryoelectron microscopy.**

INTRODUCTION

The availability of well-ordered two- or three-dimensional (3-D)[1] crystals allows protein structure to be determined by electron (Henderson *et al.,* 1990; Murata *et al.,* 2000) or X-ray crystallography (Deisenhofer *et al.,* 1984), respectively. However, such crystals are difficult to obtain, especially for membrane proteins. An alternative is to analyze electron microscopy images of randomly oriented protein particles (Orlova *et al.,* 1996). In this case, image-averaging procedures (Frank *et al.,* 1978; van Heel and Frank, 1981) improve the signal-to-noise ratio allowing resolutions between 5 and 10 Å to be obtained (Bottcher *et al.,* 1997; Conway *et al.,* 1997; Matadeen *et al.,* 1999; van Heel *et al.,* 2000). The technique has been widely applied to negatively stained samples (Frank *et al.,* 1982; Phipps *et al.,* 1993; Sato *et al.,* 1998) and in more recent years to cryoelectron microscopy (cryo-EM) images where the contrast between protein and ice is minimal (Radermacher *et al.,* 1994; Serysheva *et al.,* 1995; Sato *et al.,* 2001). The selection of a large number of particles from the micrographs is a prerequisite for success. For example, more than 10 000 images of an asymmetric 200-kDa protein had to be manually selected from cryo-EM micrographs to obtain the structure to 19 Å (Sato *et al.,* 2001). Clearly the use of an automated particle pickup algorithm would allow this tedious and rather subjective procedure to be avoided.

Several particle detection algorithms have been devised (Frank and Wagenknecht, 1984; Lata *et al.,* 1995; Thuman-Commike and Chiu, 1996; Boier Martin *et al.,* 1997; Ludtke *et al.,* 1999). These methods are classified into three types: the first is a cross-correlation method with reference images (Frank and Wagenknecht, 1984; Thuman-Commike and Chiu, 1996; Ludtke *et al.,* 1999); the second is a combination method of convolution with a Gaussian function and discriminant analysis (Lata *et al.,* 1995); and the third is a cross-point method (Boier Martin *et al.,* 1997). The correlation methods have been used mainly to select highly symmetrical virus or large protein particles. Accordingly, a reliable reference could be obtained by symmetrization. They showed few results applied to detect asymmetric particles. In this case, multireferences corresponding to the particle rotated at various Euler angles must be employed. The weak signals arising from small asymmetric proteins with masses between 100 and 300 kDa are difficult to detect by such methods. However, the structure of exactly these proteins is frequently of prime importance for fundamental biology as well as for applications such as drug development. In the present paper we report the development of a reference-free, high-precision

[1] Abbreviations used: 3-D, three-dimensional; cryo-EM, cryoelectron microscopy; NN, neural network; SD, standard deviation; TEM, transmission electron microscopy.

1047-8477/01 $35.00

particle recognition and pickup procedure that is applicable to small asymmetric proteins. It is based on the neural network (NN) system (Rosenblatt, 1961; Minsky and Papert, 1969; Rumelhart *et al.*, 1986), a powerful algorithm that has solved many pattern recognition problems (Kammerer and Kupper, 1990; Hasegawa *et al.*, 1996) including oral language recognition (Trentin and Gori, 2001). The NN has many types of network structures and algorithms (Ritter *et al.*, 1992). We find that the three-layer pyramidal-type structure with the back-propagation algorithm accomplishes high-recognition accuracy in the pickup task.

MATERIALS AND METHODS

Purification of the sodium channels and electron microscopy. The extraction of voltage-sensitive sodium channels from the electric organ of *Electrophorous electricus* eels and their purification have been described previously (Sato *et al.*, 1998, 2001). The images recorded from negatively stained samples using a Hitachi H7000 electron microscope at an acceleration voltage of 100 kV (Sato *et al.*, 1998) and from unstained cryo samples using a JEM3000SFF electron microscope at an acceleration voltage of 300 kV (Fujiyoshi, 1998; Sato *et al.*, 2001) were used to test the NN method. The pixel size of the micrographs was 6.25 and 2.83 Å, respectively, and the applied underfocus values for cryo samples ranged from 3.7 to 7.6 μm.

Construction of the NN. A multilayer NN consists of three types of layers: an input layer, a hidden layer, and an output layer (Fig. 1). We designated a pyramidal-type neural network structure, in which the units in each layer consist of 1600 or 1024 units (input layer), 81 units (hidden layer), and 1 unit (output layer). The units of the input layer receive the corresponding pixel density of the input image. In this process, the real calculations were done on simplified one-dimensional lined units instead of the two-dimensional arrayed units. Thereby, the information is simplified by the conversion of the input image data of the two-dimensional array into that of a one-dimensional input unit line. Each unit of the input layer has a linear function at the output. Therefore, outputs of the units are equal to the received input pixel densities:

$$y_{\text{inp}}(i * N + j) = p_{i,j}. \tag{1}$$

Here, $p_{i,j}$ is the input pixel density of an image, whereas y_{inp} is the output of the input layer unit. i and j are the lateral and horizontal positions of the input images, respectively.

N is the lateral and/or horizontal size of the input image (in this case 40 or 32) and $(i * N + j)$ is the linear position of its output. In the equations, generally y means output, whereas x means input of a unit.

In the next hidden layer, every unit in the hidden layer receives weighted inputs from all units in the input layer

$$x_{\mathbf{hid}(l)} = \sum_{k=1}^{N \cdot N} w_{\text{hid}(l,k)} \cdot y_{\text{inp}(k)} + w_{\text{ave}(l)} \cdot \bar{p} + \theta_l \tag{2}$$

$$\bar{p} = \frac{1}{N^2} \sum_{i=1}^{N} \sum_{j=1}^{N} p_{i,j} \tag{3}$$

$$\theta_l = w_{\text{bias}(l)} \cdot 1 \tag{4}$$

where $x_{\text{hid}(l)}$ is the total input of a hidden layer unit from the input layer units and from the average and bias unit, $w_{\text{hid}(l,k)}$ is the weight between the hidden layer and the input layer unit, and $W_{\text{ave}(l)}$ is the weight between the hidden layer and the average of the input image ($\bar{p}$). θ_l is a bias input, and it can be considered equivalent to its weight (w_{bias}) because the output of the bias unit is always 1. k is a position in the input layer units, whereas l is a position in the hidden layer units. The hidden layer units have a sigmoidal function at the output:

$$y_{\text{hid}(l)} = \frac{1}{1 + \exp(-x_{\text{hid}(l)})}. \tag{5}$$

While each unit in the input layer transmits signals to all units in the hidden layer, each unit of the hidden layer uses a single output to transmit its information further to an output layer unit. The NN output (y_{out}) was calculated using the following equations:

$$x_{\text{out}} = \sum_{l=1}^{L} w_{\text{out}(l)} \cdot y_{\text{hid}(l)} + \theta_{\text{out}} \tag{6}$$

$$\theta_{\text{out}} = w_{\text{bias(out)}} \cdot 1 \tag{7}$$

$$y_{\text{out}} = \frac{1}{1 + \exp(-x_{\text{out}})}. \tag{8}$$

Similarly x_{out} is the total input of an output unit. $w_{\text{out}(l)}$ is the weight between the output layer and the hidden layer, and θ_{out} is the bias input to the output layer. L is the total number of hidden layer units (9×9 units). The back-propagation algorithm adjusts the connection weights ($w_{\text{hid}(l,k)}$ and $w_{\text{out}(l)}$), offset weights ($w_{\text{bias}(l)}$ and $w_{\text{bias(out)}}$), and weights of the input image average ($W_{\text{ave}(l)}$).

The three-layer NN employed was constructed to achieve automatic particle selection independent of a predefined reference. The outputs from each unit in the hidden layer and from the single unit of the output layer were sigmoidal functions of their total inputs. A bias of 1 could be weighted and applied to the inputs of all hidden and output layer units. Weights initially ranging from -0.5 to 0.5 at first allowed the signals transferred between the three layers to be adjusted during the training process by a back-propagation algorithm (Rumelhart *et al.*, 1986). The average intensity of the input layer was also calculated. Adjustment of the information to the hidden layer via an average unit enabled robust particle detection regardless of shifts in the individual input image averages. The number of neurons used in the input layer depended on the size of the particles to be recognized. In the present case, 32×32 and 40×40 units were required to detect particles on the negatively stained and cryo-EM micrographs, respectively; 9×9 units were adopted for the hidden layer for both types of images.

Image processing. The intensities of the input digital images to the NN were normalized to values between 0 and 1 to match the output value range and to eliminate the gap of average intensity of each EM image. For the negative stain images the average value of the entire EM image intensity was first subtracted from each pixel. After the addition of 256, the pixel values were then divided by 512. The sizes of the cryo-EM images were reduced by half before 2D normalization and a high-pass filter

was applied (31 × 31 pixels; cut-off frequency 0.05). For normalization, after subtraction of the average image intensity from the entire image, 4 times the SD was added. Each pixel value was then divided by 8 times the SD. Since these image processings are linear conversions, the resulting particle images have shifts only in the distributions of their pixel densities.

Learning process. The learning process of the NN consisted of repeatedly presenting input and output data to the network whereby the actual output was compared to the desired output using a back-propagation algorithm. The NN learned the negatively stained images or cryo-EM images to produce a specific NN recognition system for the pickup task. In this process, 200 particle images were manually selected from each micrograph set to serve as a positive learning data set (desired output 1). The 200 particle images are divided into four groups of 50 images each (Fig. 2). The required negative learning data set (desired output 0) was created from two different kinds of artificial random noise, normally distributed and uniformly distributed random noise (Fig. 2, bottom right), in order to improve the recognition accuracy. The normally distributed noise parameter was set to a mean value of 0.45–0.55 and to a SD of 0.2. The uniformly distributed noise images were set to a brightness range between 0.25 and 0.75. Each learning data set was a mixture of the single-particle image rotated at 90° increments to create four images, two normally distributed noise images and two uniformly distributed noise images (Fig. 2, bottom).

For the training process, the density of each pixel of an input image was read to a corresponding input layer neuron whereby the desired output was set to 1 for each interactively selected particle image indicating correct data and to 0 for each random noise image indicating incorrect data. The average value of the input layer was also calculated and transferred to an average unit and further to the hidden layer. The weights used to transfer information between individual neurons of the input, hidden, and output layers were initially randomly but uniformly distributed between −0.5 and 0.5. They were adjusted after each new input image by back-propagation, which compares the output with the desired result, being changed by a learning rate of 0.05 toward the direction to minimize the sum of the squared errors until the optimum value had been attained (Rumelhart *et al.*, 1986).

In the first training step a learning data set of 400 learning images (200 rotationally created single-particle images and 200 noise images) was repeatedly presented to the NN until the average mean square error was 0.01–0.003. To optimize the network weighting further, a new set of 400 learning images was then presented and the procedure repeated and so on until all 200 particle learning images had been included (four cycles). The whole 4-step cycle (one turn) was further repeated 20 times using the same particle images and newly generated noise images (Fig. 3a). In total 16 000 noise images were employed for the training.

Pickup procedures. The recognition and selection of particle images in the large area of an electron micrograph were done in three steps: (1) A square area of defined size was extracted from the micrograph. (2) Either its correlation with the references (cross-correlation method), fitted to the Gaussian peak, or its NN output (NN method) was calculated and the values were entered on the corresponding map. Steps (1) and (2) were repeated, shifting the square region by one pixel until the whole micrograph had been scanned and mapped. Finally, (3) the maxima on the map were identified and the corresponding square regions extracted from the original micrograph.

Image analysis system. All filtering and NN learning processes were performed with the image-processing toolbox of Matlab Version 6 (MathWorks, Inc.) on a personal computer running Windows 98 (Pentium III, 800 MHz, 512 Mb RAM). The three-layer NN was programmed using the Matlab script M-files.

RESULTS

A flow diagram outlining NN learning and automated particle recognition and pickup procedure which we have developed is shown in Fig. 1a. A three-layer NN structure was adopted (Fig. 1b). In the first step, examples of the randomly oriented protein particles are manually selected from the filtered electron micrographs. The learning data set for one cycle was a mixture of the rotated particle images and artificially generated random noise images (Fig. 2). This learning data set was employed for the neuronal learning process (see Materials and Methods), which consists of repeatedly presenting learning data sets to the network and comparing the output from the output unit with the desired output by back-propagation until the best connection weights among the three layers have been defined (Fig. 3a). For this process, outputs of 0 and 1 define the images as noise or particle, respectively. A learning error is increased by the replacement of the learning data set and decreased by the repeated learning of one data set. Therefore, the time course of the learning error exhibits a curve just like the teeth on a saw (Fig. 3b). After training, the NN contains the features of the particle structure in terms of the connection weights employed on reading the input data into the central hidden layer. That is, interpreting these connection weights as pixel densities, the two-dimensional shapes stored in the connections (recognition images; Fig. 3c) are comparable to average projections of the single particle viewed at various Euler angles (reported in Sato *et al.*, 1998, 2001).

The accuracy of the NN method of particle pickup is compared to that of conventional correlation techniques in Fig. 4. The same particle and background noise images interactively selected from micrographs of sodium channel proteins were analyzed by the two techniques, the NN method and the cross-correlation particle recognition method. In both cases they were distinguished when they arose from negatively stained samples as documented by the traces and histograms shown in Fig. 4a. The correlation values of the particle and noise images from these high-contrast micrographs range from 0.26 to 0.78 and from 0.09 to 0.35, respectively, and the two histogram peaks can be separated at a 0.32 border value. However, particles and noise were even more precisely distinguished by the NN procedure. The results are distributed into sharp peaks at 1 (particle) and 0 (noise) showing NN recognition to be extremely reliable. In contrast, only the NN method was able to reliably distinguish between the channel particles and background noise on the low-contrast micrographs recorded from unstained samples by

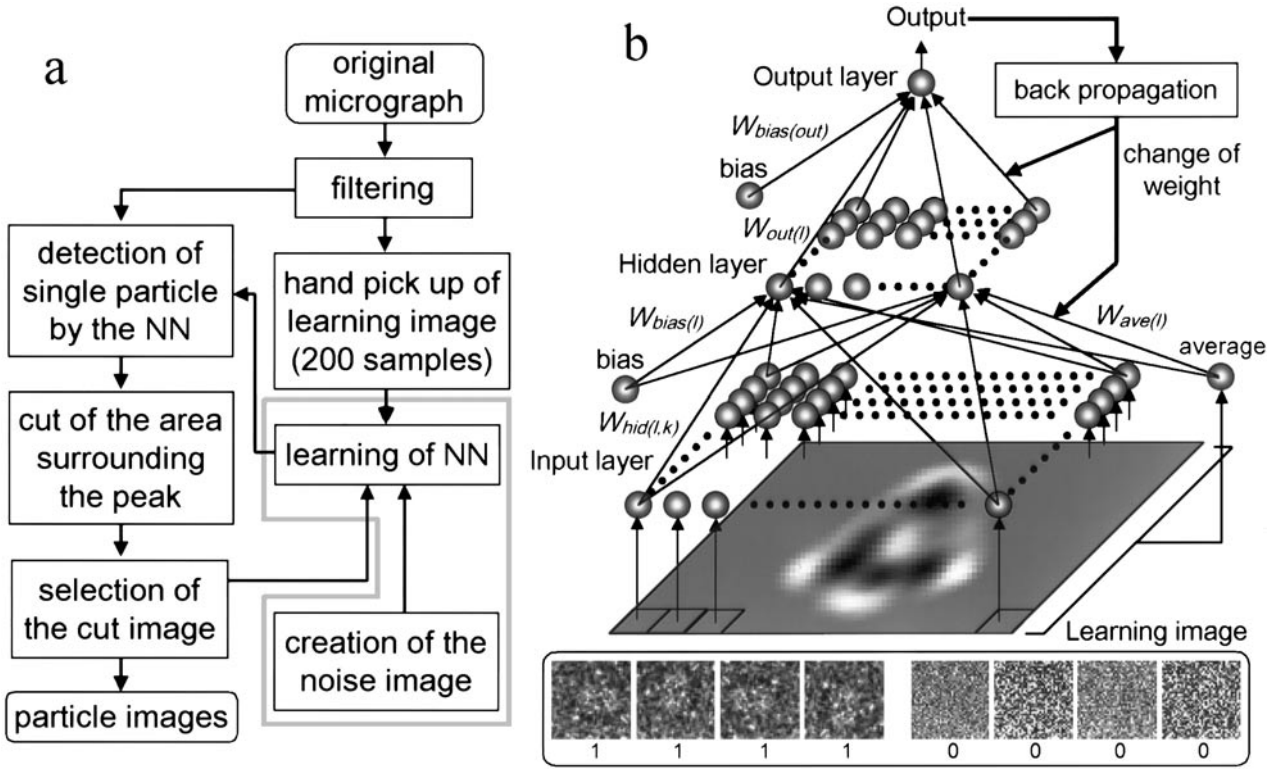

FIG. 1. NN particle picking. (a) Flow diagram outlining the learning and automated particle pickup procedure. The learning process surrounded by the gray line is shown in more detail in Fig. 3a. (b) Schematic representation of the three-layer NN and its learning process. The learning and recognition images are read into and set in the input layer and propagated to the next layer by the connection weights between the units. The connection weights are adjusted by the back-propagation algorithm to minimize the difference between the actual output and the desired output. The unit shown to the left of the input layer is the bias and to the right the average. The former has the value 1 and the latter is the average value of the input image. The unit shown to the left of the hidden layer also has a bias of value 1 and is weighted similarly and transmitted to the output. Examples from a typical micrograph learning set are shown in the inset.

cryo-EM, as shown in Fig. 4b. In this case the correlation values obtained for particle and noise images are almost identical, whereas NN analysis still yields a comparatively clear-cut result. Although there is a margin of uncertainty, 59.2% of all particle images and 95.0% of all noise images are correctly distinguished when the border value is taken to be 0.74 on the output scale.

The selection accuracies of the NN and cross-correlation particle recognition methods when applied to scan micrographs of negatively stained sodium channel proteins are compared in Fig. 5. The correlation method, using average images as references, yielded a correlation map with a distribution of low peaks surrounded by comparatively high background noise (Fig. 5a). Almost all particles were recognized (Fig. 5b). The output map from the NN method (Fig. 5c) exhibited well-defined peaks above almost zero background, making particle recognition very efficient (Fig. 5d). Furthermore, the convolution method with a Gaussian function, where the width is set to fit the diameter of the sodium channel, showed a smooth undulating image (Fig. 5e). Its peak points are biased in certain areas and correspond to the background noise in most cases (Fig. 5f). Therefore, the result is even worse than the correlation method and the NN method.

This difference from the correlation map is illustrated by the histograms displayed in Fig. 5g. While the correlation values have a normal distribution, the NN map densities form a sharp peak at zero with a long tail toward positive values. A significant difference between the two methods is illustrated by their detection of the protein dimer present in the micrograph shown in Fig. 5. While this is recognized as a single particle by the correlation method (Figs. 5b and 5h, middle), NN analysis correctly detects the presence of two protein particles (Figs. 5d and 5h, right).

The selection accuracies were similarly tested using low-contrast cryo-EM images of unstained sodium channel proteins. The correlation maps exhibited high background noise above which the faint maxima corresponding to particles could not be re-

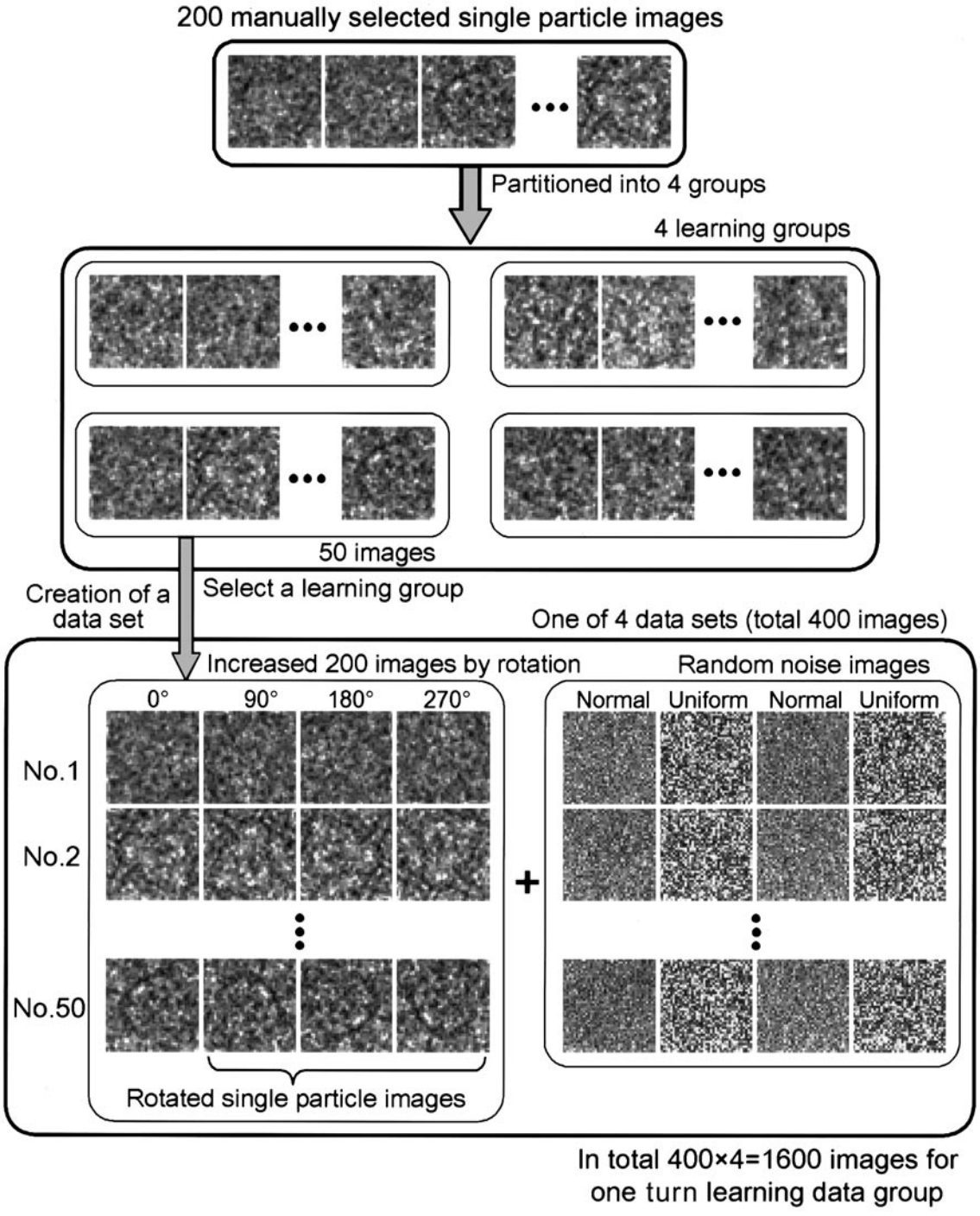

FIG. 2. A schematic diagram for the creation of a learning data set. It was created basically from 200 manually selected single-particle images, which were partitioned into four groups. The 50 single-particle images in a group were rotated clockwise 90°, 180°, and 270°, to create 200 images. Each learning data set was a mixture of the rotated images, 100 normally distributed noise images, and 100 uniformly distributed noise images. A learning data group contains 1600 images in total.

liably distinguished (Fig. 6a). Indeed, even those regions with the highest correlation values frequently contained only noise (Fig. 6b; $n = 20$). NN analysis of the same images resulted in maps exhibiting many clear peaks (Fig. 6c). Regions yielding output values above 0.98 ($n = 20$ for Fig. 6c) were recognized as particles. When examined, 95% of these regions were found to contain well-defined

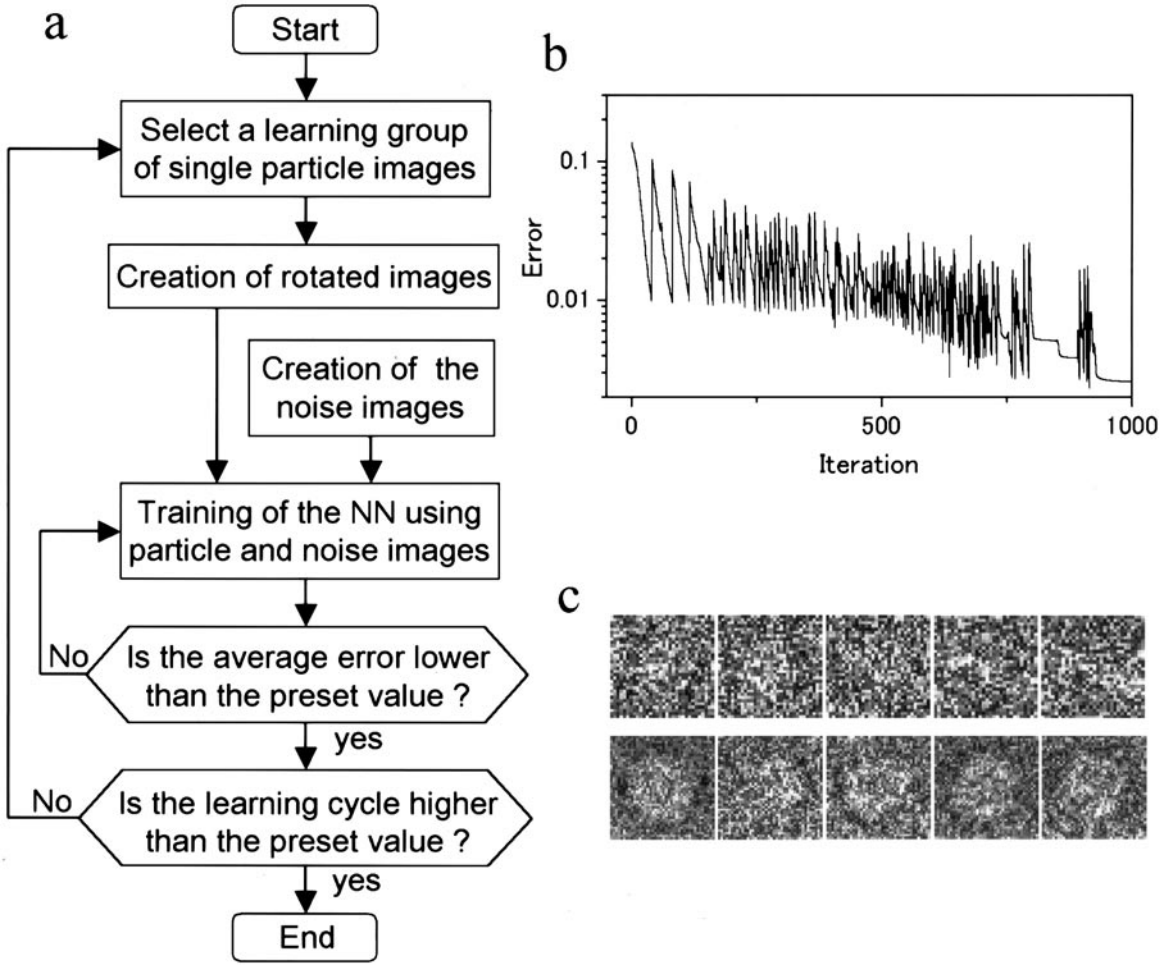

FIG. 3. Detail of the learning process and the features of the particle stored in terms of connection weights. (a) A flow chart of the primary learning process of the NN. The flow chart shows details of the part surrounded by the gray line in Fig. 1a. (b) The changes of the sum of the squared errors at learning cycles. In total, the errors are decreased gradually by repeated learning; however, the replacement of a learning data set increases it temporarily. (c) Examples of visualized features of the two-dimensional filters stored in terms of connection weights between the hidden and input layers after the training (20 turns). Each image represents the connection weights of the hidden unit from the input layer units. Those in the upper panels arise from negatively stained protein particles and those in the lower panels from the unstained protein particles by cryo-EM.

particles (Fig. 6d). This was similar for a further five images; between 90 and 95% of the regions with output values above 0.98 contained well-defined particles. For the micrograph shown in Fig. 6, only four regions corresponded to regions picked by the correlation method (Fig. 6d, asterisks). Further, the convolution method with the Gaussian function showed several broad peak points (Fig. 6e). These peak points included several good particles (Fig. 6f). The selection accuracy was not as good as the NN and almost similar to that of the correlation method.

Five examples of particles picked up by the NN method are shown in Fig. 6g together with corresponding views of the current 3-D model (Sato *et al.*, 2001). The comparative robustness of the NN method is documented by the histograms shown in Fig. 6h. Again the correlation values have a normal distribution with a short tail. Although the NN map densities are distributed over the whole range, there are sharp peaks at 0 with a long tail toward 1 arising from regions clearly identified as noise and particles, respectively.

As a final test, a cryo-EM image of a thin ice layer without single particles (Fig. 7a) was examined by both methods. Back projections of the sodium channel model were used as references for the cross-correlation (Fig. 7b). The resulting map was very similar to that shown in Fig. 6a, which was calculated for a cryo-EM micrograph where particles were present. This confirms that in the cross-correlation, regions selected as particles generally just contained background noise. Indeed, the highest correlation

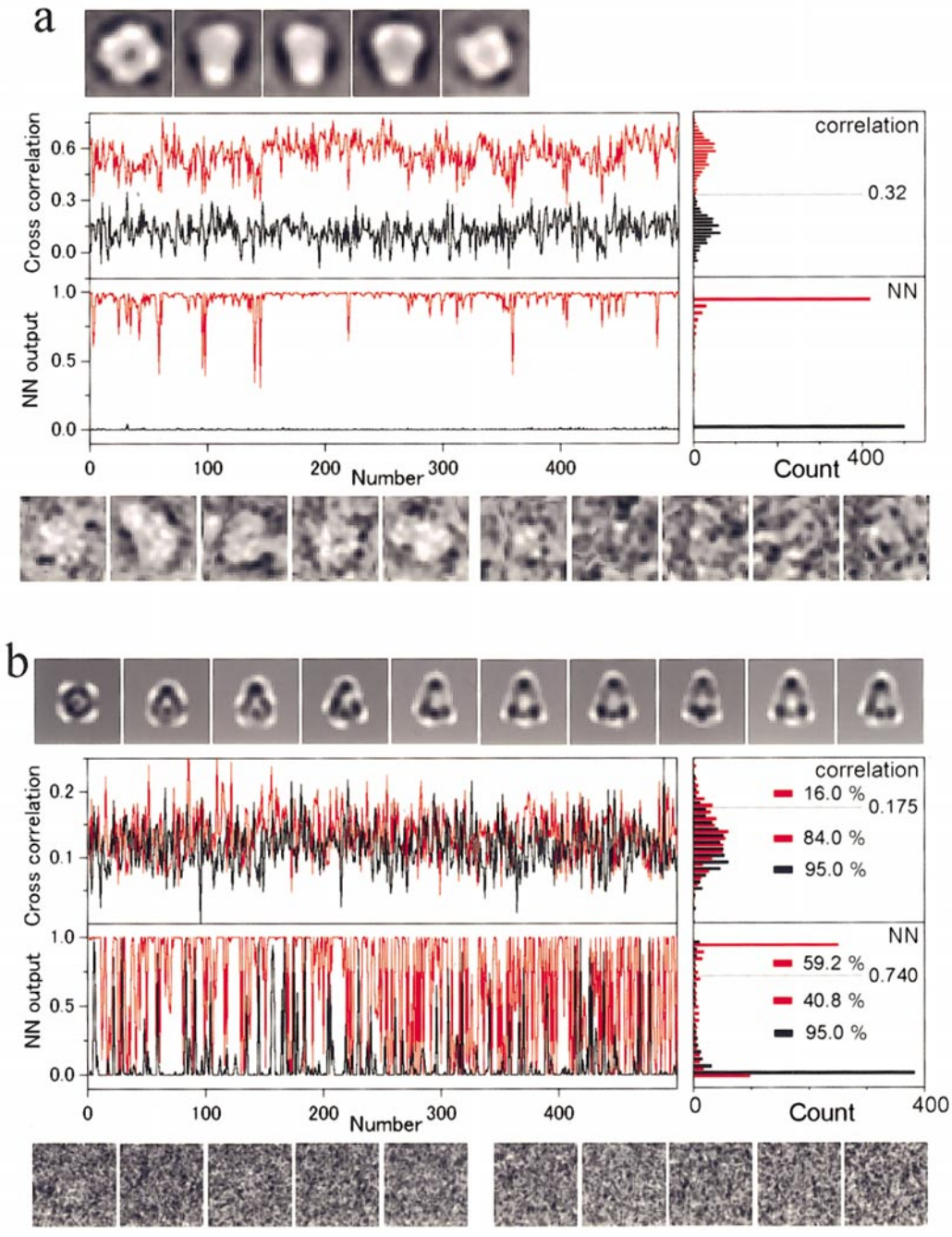

FIG. 4. Ability of the NN and cross-correlation methods to distinguish between single particles and background noise. Both analysis methods were applied to 500 particle images and 500 background noise images interactively selected from the micrographs. (a) Results for micrographs of negatively stained sodium channels obtained by conventional transition electron microscopy. The five average projection images shown (Sato *et al.*, 1998) (top left) were rotated clockwise through 360°, by 2° increments to provide a total of 900 reference images for the cross-correlation. The graphs display the maximum cross-correlation value and NN output for each particle (red lines) and background noise (black lines) image. The *x*-axis indicates the image sequence. Histograms of the outputs are shown on the right. Here, the *x*-axis indicates the total number of images with a given value. Although the cross-correlation method can distinguish between particles and background noise the NN method is clearly the more reliable. (Bottom left) The 5 images with the highest NN values (0.996–1.0); the particles are well defined. (Bottom right) The 5 particle images with the lowest NN values (0.306–0.403); the particles are difficult to distinguish. (b) Results for micrographs of unstained sodium channels obtained by cryo-EM. Data as in (a) except that the 10 references shown were the projections of the model (Sato *et al.*, 2001) and rotated clockwise through 360° by 2° increments to generate 1800 references for the cross-correlation. From the histograms it is quite clear that while particles and noise are not distinguishable by cross-correlation they are still reliably separated by the NN method. (Bottom left) The 5 images with the highest NN values (1); the particles are visible. (Bottom right) The 5 particle images with the lowest NN values (0); the particles are barely distinguishable.

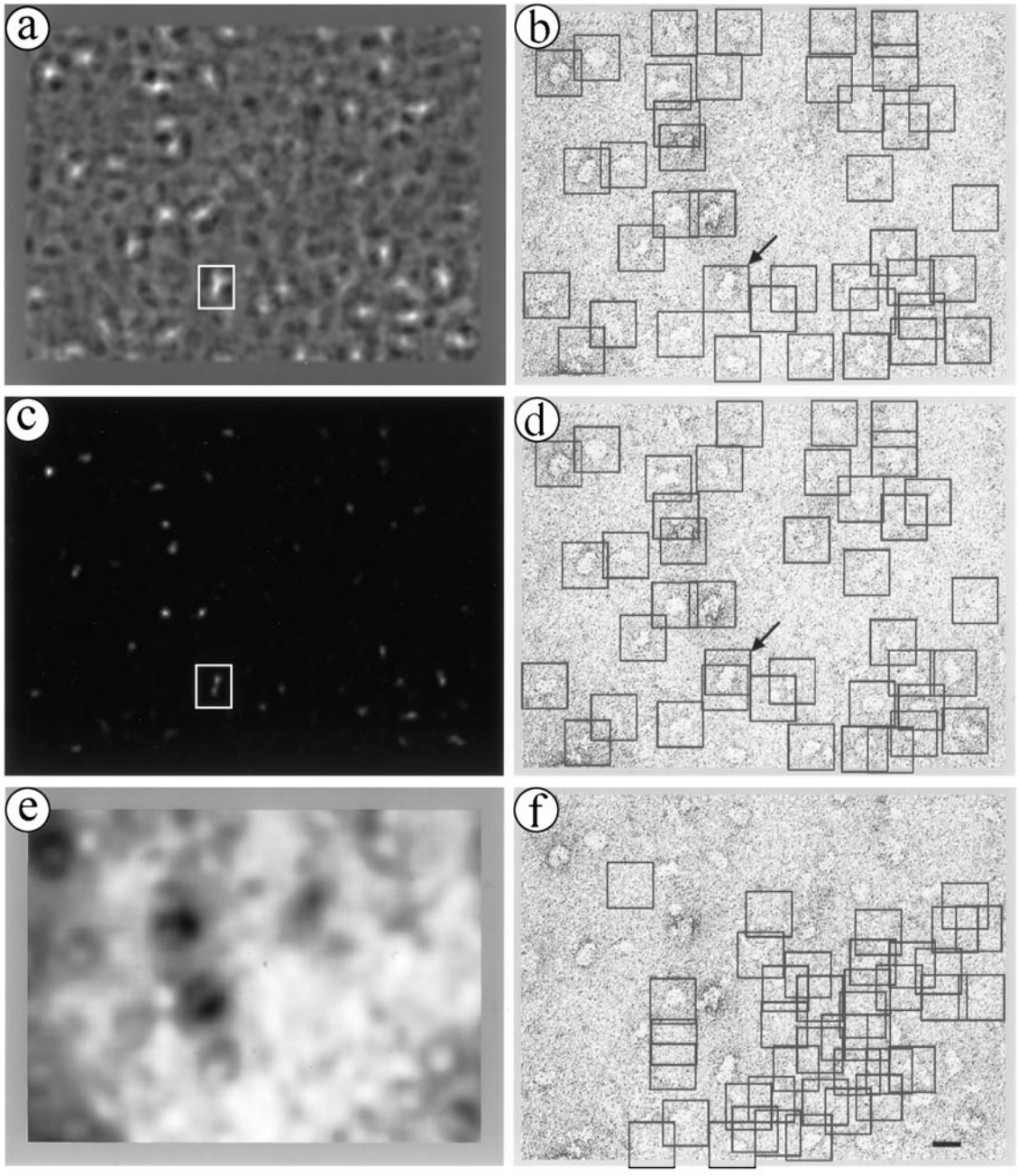
a
b
c
d
e
f

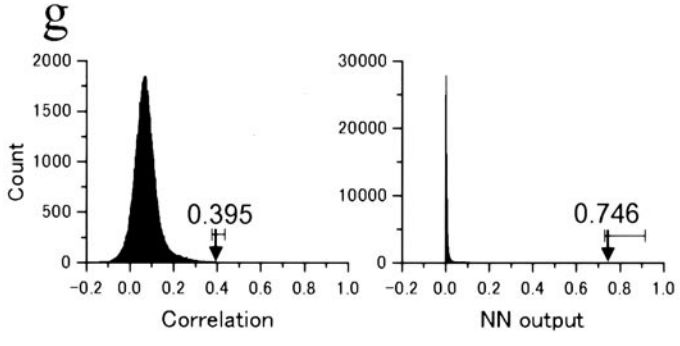
g
Count
2000
1500
1000
500
0
0.395
-0.2 0.0 0.2 0.4 0.6 0.8 1.0
Correlation
30000
20000
10000
0
0.746
-0.2 0.0 0.2 0.4 0.6 0.8 1.0
NN output

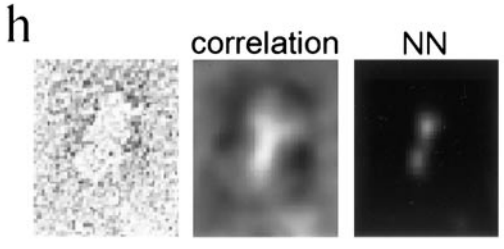
h
correlation
NN

found in the absence of particles was 0.219 (Fig. 7d) and in their presence 0.227. This small difference of 3.5% proves that most of the signal arising from particles overlaps with that arising from noise (as already demonstrated in Fig. 4b), making the two almost impossible to distinguish by this method. The NN output map for the empty ice layer (Fig. 7c) is markedly different from that obtained when particles are present (Fig. 6c). Accordingly its maximum value was only 0.453 compared to the 1.0 value obtained when particles were present. This large difference, 54.7%, means that particles can be reliably distinguished from background noise.

In general, increasing the electron accelerating voltage and decreasing the amount of defocus used to record micrographs increases their resolution. However, under these conditions contrast is decreased, making small proteins such as 200-kDa sodium channels even more difficult to discern on cryo-EM micrographs. However, after learning from images recorded at large defocus, the NN could also recognize such particles on micrographs recorded at 1-μm defocus with an omega filter to decrease background noise (data not shown).

DISCUSSION

At present, the resolution achieved by single-particle analysis is limited by the number of projection images available and the generally large defocus used to record them. Particle recognition and selection programs are indispensable tools. However, a recognition program capable of reliably detecting symmetric and asymmetric protein particles even when these are imaged at extremely low contrast is lacking. As illustrated by the results presented, the NN recognition method can fill this gap. Comparison with the widely used, reference-dependent cross-correlation technique (Frank and Wagenknecht, 1984; Thuman-Commike and Chiu, 1996; Ludtke *et al.*, 1999) showed the NN method to be superior under all of the conditions tested. In this essentially reference-free method, particle images interactively selected by the operator and presented to the NN together with artificially generated noise images train the NN to identify the features of a particle.

In the NN method the connection weights assigned to the particle featured during training work as template-matching filters, allowing particle recognition. The better the signs of the pixel densities match those of the connection weights, the larger the input into the hidden unit becomes. In the present study, the NN makes 81 template-matching filters (groups of connection weights) since 81 hidden units were adopted. The connection weight between the hidden layer and the output layer acts as a mixer of each output created by the template filter matching. Thereby, a limited number of template-matching filters of 81 seems to work well even on a particle projection of the intermediate Euler angle from that of the filters. For the number of the unit in the hidden layer of the NN, 81 seems accurate enough to pickup the present pseudo-fourfold symmetric sodium channel. Thus, the net weight of the layers defines image fields as particles or noise and indicates the precision of the assignment; the closer the value is to +1, the better the match to the particle templates. This higher precision of the NN is most likely due to the automatically designed many matching filters and to the sigmoidal functions for the hidden and output layers. After the initial learning process, training of the NN can be continued as required and the selection accuracy improved by using further training data sets comprised of automatically picked particles. Although the initial interactive selection of the required number of particle images (approximately 200) is time-consuming, it is more objective than creating a reference from a small number of the faint images of small proteins obtained by cryo-EM.

The detection accuracy of the convolution method with a Gaussian function decreased when it was stained. The accuracy of this method seems to be

FIG. 5. Selection accuracy of the NN and cross-correlation particle recognition methods when applied to micrographs of negatively stained proteins. (a) Typical correlation map obtained using the 900 references generated by rotating five average projection images (Fig. 4a) clockwise through 360° by increments of 2°. A mean filter of 5 × 5 was applied to aid recognition. The white square indicates the position of a protein dimer. (b) Particle selection on the corresponding micrograph. The selected particles, marked by squares, correspond to the 40 highest peaks on the map. The arrow indicates the protein dimer that correlated as a single particle. (c) Output map obtained from the same micrograph by the NN method. A mean filter of 5 × 5 was applied. Particles appear as well-defined bright spots, two of which indicate the position of the dimer (white square). (d) Particle selection by the NN method. As in (b) the 40 highest peaks on the map were used. The selected particles are marked by squares. Most correspond to those selected by cross-correlation. However, in this case the protein dimer is selected as two monomers (arrow). (e) Output map obtained from the same micrograph by the convolution method with a Gaussian function. The width of the Gaussian function fits the particle size (20 pixels). (f) Particle selection by the convolution method. The selected areas are almost without particles. The scale bar represents 200 Å. (g) Histograms of the maps shown in (a) and (c). The correlation values form a normal distribution (left), whereas the NN map densities (right) give rise to a sharp peak at zero with a long tail toward positive values. The arrows indicate their maximum values and the error bars the variation (standard deviation, SD) of the maximum values of these and a further five maps. (h) The protein dimer and its detection by the correlation and NN methods.

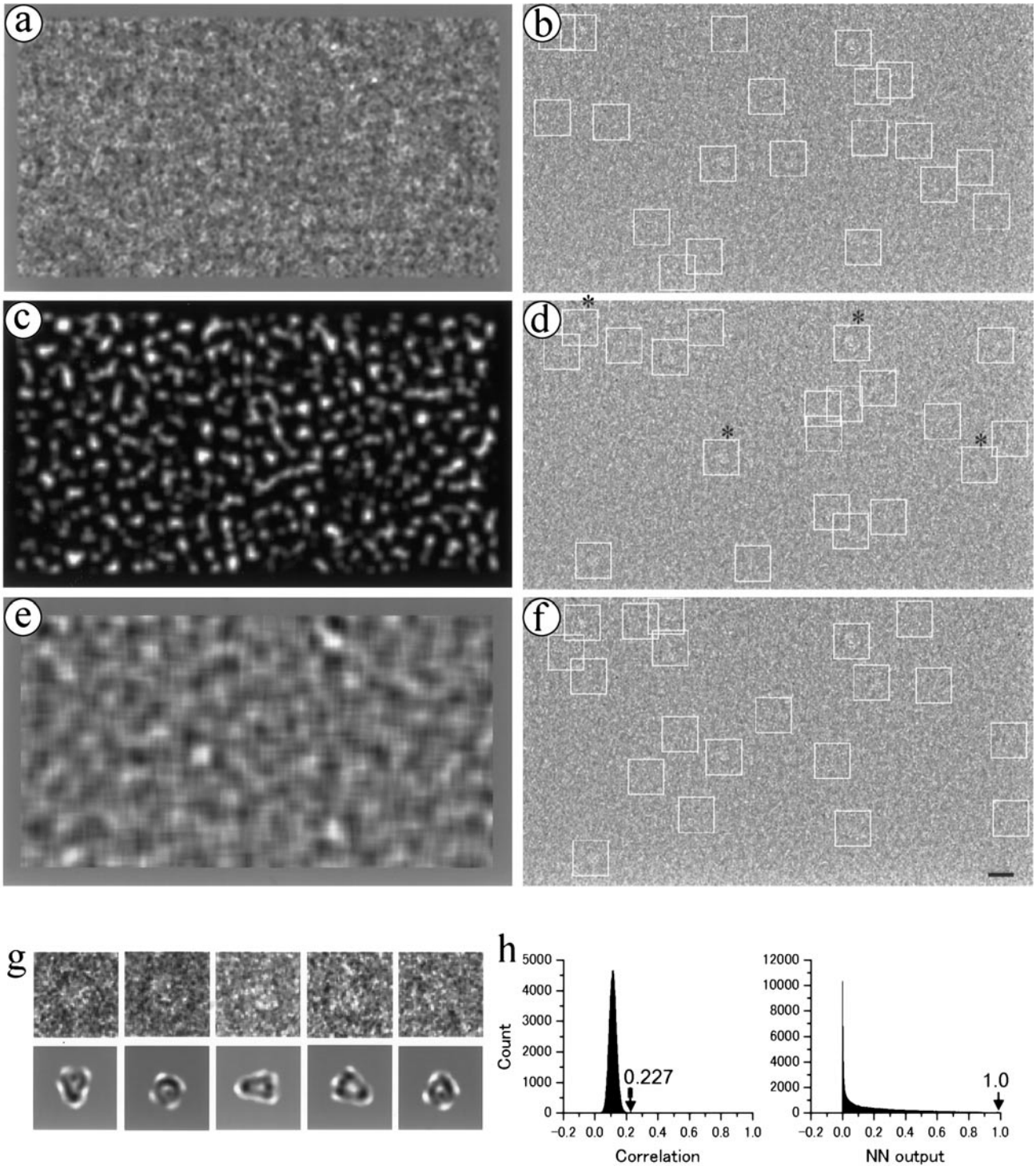

FIG. 6. Selection accuracy of the NN and cross-correlation particle recognition methods when applied to micrographs of unstained sodium channels recorded by cryo-EM. (a) Typical correlation map obtained using 1800 references generated by rotating 10 average density images (Fig. 4b) clockwise through 360° by increments of 2°. A median filter of 3 × 3 was followed by a mean filter of 5 × 5 to aid recognition. (b) Particle selection on the corresponding micrograph. The selected particles, marked by white squares, correspond to the 20 highest peaks on the map, which has a maximum value of 0.227. (c) Output map obtained from the same micrograph by the NN method. A median filter of 7 × 7 was followed by a mean filter of 9 × 9 to minimize the effect of very sharp erroneous peak which is rarely observed in the background noise (Fig. 4b, lower NN traces). (d) Particle selection by the NN method. As in (b) the 20 highest peaks on the map were used; map maximum 1.0. The selected particles are marked by white squares. Only a few of the regions (marked with asterisks) are the same as those selected by cross-correlation. (e) Output map obtained from the same micrograph by the convolution method with a

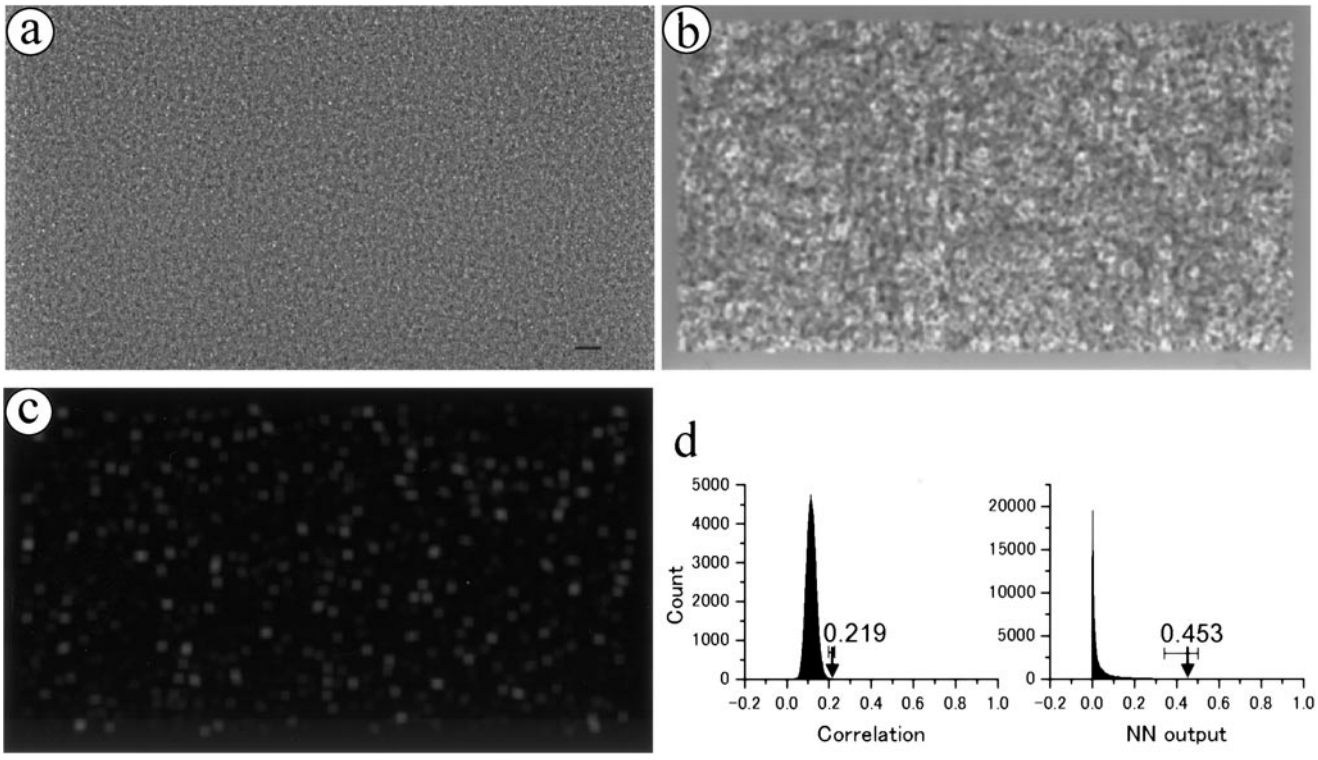

FIG. 7. Selection accuracy of the NN and cross-correlation particle recognition methods when applied to a micrograph of thin ice alone (no protein sample) recorded by cryo-EM. (a) The test micrograph. The scale bar represents 200 Å. (b) Correlation map obtained using the 1800 references generated for sodium channel recognition on cryo-EM micrographs. As in Fig. 6a, a median filter of 3×3 was followed by a mean filter of 5×5 to aid recognition. Note the marked similarity of the two maps. (c) Output map obtained by the NN method. As in Fig. 6c, a median filter of 7×7 was followed by a mean filter of 9×9. The two maps bear little similarity to one another. (d) Histograms of the maps shown in (b) and (c). The correlation values form a normal distribution with a short tail (left), whereas the NN map densities (right) give rise to a sharp peak at zero with a tail toward positive values. The arrows indicate their maximum values and the error bars the variation (SD) of the maximum values of these and a further five corresponding maps.

easily influenced by the high background noise created by the staining. Furthermore, the failure to detect a particle image by this method might be due to the special internal structure of the sodium channel since it has a central core surrounded by an internal cavity and further by an outer shell (Sato *et al.*, 2001).

The single-particle images adopted for the training are the projections of a sodium channel which is oriented almost randomly (Sato *et al.*, 2001). Therefore, the present NN pickup method works best when the user arbitrarily picks up enough single particles in the EM image. When the user factitiously chose a certain kind of single-particle image of a certain Euler angle, the NN had a tendency to show a biased selection, too (data not shown). However, we think this shortcoming has the possibility of becoming an advantage, since the bias could lead to the classification of single-particle images during the pickup task by selected learning data. Certainly some kinds of proteins are known to possess a biased particle direction in the thin buffer layer formed in a holey carbon grid. In such a case, more learning images would be required to cover various Euler angles.

In conclusion, the NN particle pickup method provides a much-needed tool that allows fast and reliable particle recognition of images recorded at a

Gaussian function. The width of the Gaussian function fits the particle size (24 pixels). (f) Particle selection by the convolution method. The scale bar represents 200 Å. (g) Five particles selected by the NN method (top) together with corresponding views of the current 3-D model (Sato *et al.*, 2001) (bottom). (h) Histograms of the maps shown in (a) and (c). The correlation values form a normal distribution with a short tail (left), whereas the NN map densities (right) give rise to a sharp peak at zero with a long tail toward positive values. The arrows indicate their maximum values and the error bars the variation (SD) of the maximum values of these and a further five corresponding maps.

lower defocus condition required for higher resolution of smaller particles.

The authors express their cordial thanks to Dr. Shirley Müller (MIH, Biozentrum, Basel, Switzerland) for her illuminating suggestions and help with the manuscript, to Dr. Yoshinori Fujiyoshi (Kyoto University, Japan) for cryomicroscopy and discussions, and to Dr. Andreas Engel (MIH, Biozentrum, Basel, Switzerland) for his suggestions. This work was supported by a grant from the Japan New Energy and Industrial Technology Development Organization (NEDO) and by grants from the AIST.

REFERENCES

Boier Martin, I. M., Marinescu, D. C., Lynch, R. E., and Baker, T. S. (1997) Identification of spherical virus particles in digitized images of entire electron micrographs. *J. Struct. Biol.* **120,** 146–157, doi:10.1006/jsbi.1997.3901.

Böttcher, B., Wynne, S. A., and Crowther, R. A. (1997) Determination of the fold of the core protein of hepatitis B virus by electron cryomicroscopy. *Nature* **386,** 88–91.

Conway, J. F., Cheng, N., Zlotnick, A., Wingfield, P. T., Stahl, S. J., and Steven, A. C. (1997) Visualization of a 4-helix bundle in the hepatitis B virus capsid by cryo-electron microscopy. *Nature* **386,** 91–94.

Deisenhofer, J., Epp, O., Miki, K., Huber, R., and Michel, H. (1984) X-ray structure analysis of a membrane protein complex. Electron density map at 3 Å resolution and a model of the chromophores of the photosynthetic reaction center from *Rhodopseudomonas viridis*. *J. Mol. Biol.* **180,** 385–398.

Frank, J., Goldfarb, W., Eisenberg, D., and Baker, T. S. (1978) Reconstruction of glutamine synthetase using computer averaging. *Ultramicroscopy* **3,** 283–290.

Frank, J., Verschoor, A., and Boublik, M. (1982) Multivariate statistical analysis of ribosome electron micrographs. L and R lateral views of the 40 S subunit from HeLa cells. *J. Mol. Biol.* **161,** 107–133.

Frank, J., and Wagenknecht, T. (1984) Automatic selection of molecular images from electron micrographs. *Ultramicroscopy* **12,** 169–176.

Fujiyoshi, Y. (1998) The structural study of membrane proteins by electron crystallography. *Adv. Biophys.* **35,** 25–80.

Hasegawa, A., Shibata, K., Itoh, K., Ichioka, Y., and Inamura, K. (1996) An adaptive neural network: Application to character recognition on X-ray films. *Neural Networks* **9,** 121–127.

Henderson, R., Baldwin, J. M., Ceska, T. A., Zemlin, F., Beckmann, E., and Downing, K. H. (1990) Model for the structure of bacteriorhodopsin based on high-resolution electron cryo-microscopy. *J. Mol. Biol.* **213,** 899–929.

Kämmerer, B. R., and Küpper, W. A. (1990) Experiments for isolated-word recognition with single- and two-layer perceptrons. *Neural Networks* **3,** 693–706.

Lata, K. R., Penczek, P., and Frank, J. (1995) Automatic particle picking from electron micrographs. *Ultramicroscopy* **58,** 381–391.

Ludtke, S. J., Baldwin, P. R., and Chiu, W. (1999) EMAN: Semiautomated software for high-resolution single-particle reconstructions. *J. Struct. Biol.* **128,** 82–97, doi:10.1006/jsbi.1999.4174.

Matadeen, R., Patwardhan, A., Gowen, B., Orlova, E. V., Pape, T., Cuff, M., Mueller, F., Brimacombe, R., and van Heel, M. (1999) The *Escherichia coli* large ribosomal subunit at 7.5 Å resolution. *Structure* **7,** 1575–1583.

Minsky, M. L., and Papert, S. (1969) Perceptrons, MIT Press, Cambridge.

Murata, K., Mitsuoka, K., Hirai, T., Walz, T., Agre, P., Heymann, J. B., Engel, A., and Fujiyoshi, Y. (2000) Structural determinants of water permeation through aquaporin-1. *Nature* **407,** 599–605.

Orlova, E. V., Serysheva, I. I., van Heel, M., Hamilton, S. L., and Chiu, W. (1996) Two structural configurations of the skeletal muscle calcium release channel. *Nat. Struct. Biol.* **3,** 547–552.

Phipps, B. M., Typke, D., Hegerl, R., Volker, S., Hoffmann, A., Stetter, K. O., and Baumeister, W. (1993) Structure of molecular chaperone form a thermophilic archaebacterium. *Nature* **361,** 475–477.

Radermacher, M., Rao, V., Grassucci, R., Frank, J., Timerman, A. P., Fleischer, S., and Wagenknecht, T. (1994) Cryo-electron microscopy and three-dimensional reconstruction of the calcium release channel/ryanodine receptor from skeletal muscle. *J. Cell Biol.* **127,** 411–423.

Ritter, H., Martinetz, T., and Schulten, K. (1992) Neural Computation and Self-Organizing Maps, Addison-Wesley, Reading, MA.

Rosenblatt, F. (1961) Principles of Neurodyanamics: Perceptrons and the Theory of Brain Mechanisms, Spartan Books, Washington, DC.

Rumelhart, D. E., Hinton, G. E., and Williams, R. J. (1986) Learning representations by back-propagating errors. *Nature* **323,** 533–536.

Sato, C., Sato, M., Iwasaki, A., Doi, T., and Engel, A. (1998) The sodium channel has four domains surrounding a central pore. *J. Struct. Biol.* **121,** 314–325, doi:10.1006/jsbi.1998.3990.

Sato, C., Ueno, Y., Asai, K., Takahashi, K., Sato, M., Engel, A., and Fujiyoshi, Y. (2001) The voltage-sensitive sodium channel is a bell-shaped molecule with several cavities. *Nature* **409,** 1047–1051.

Serysheva, I. I., Orlova, E. V., Chiu, W., Sherman, M. B., Hamilton, S. L., and van Heel, M. (1995) Electron cryomicroscopy and angular reconstitution used to visualize the skeletal muscle calcium release channel. *Nat. Struct. Biol.* **2,** 18–24.

Thuman-Commike, P. A., and Chiu, W. (1996) PTOOL: A software package for the selection of particles from electron cryomicroscopy spot-scan images. *J. Struct. Biol.* **116,** 41–47, doi:10.1006/jsbi.1996.0008.

Trentin, E., and Gori, M. (2001) A survey of hybrid ANN/HMM models for automatic speech recognition. *Neurocomputing* **37,** 91–126.

van Heel, M., and Frank, J. (1981) Use of multivariate statistics in analysing the images of biological macromolecules. *Ultramicroscopy* **6,** 187–194.

van Heel, M., Gowen, B., Matadeen, R., Orlova, E. V., Finn, R., Pape, T., Cohen, D., Stark, H., Schmidt, R., Schatz, M., and Patwardhan, A. (2000) Single-particle electron cryo-microscopy: Towards atomic resolution. *Q. Rev. Biophys.* **33,** 307–369.